Investigation of slope instability induced by seepage and erosion by a particle method

Investigation of Slope Instability induced by Seepage and Erosion by a Particle Method

Johan Vandamme[1]*; Qingping Zou[2]

[1] School of Architecture, Design & the Built Environment, Nottingham Trent University, Burton Street, Nottingham NG1 4BU, UK E-mail: johan.vandamme@plymouth.ac.uk
[2] Department of Civil and Environmental Engineering, University of Maine, Orono, Maine 04469, USA E-mail: qingping.zou@maine.edu

Abstract

A novel particle based Bluff Morphology Model (BMM) developed by the authors is extended in this paper to investigate the effect of two dimensional seepage on the stability and collapse of soil slopes and levees. To incorporate the seepage in the model, Darcy's law is applied to the interactions among neighbouring soil particles and ghost particles are introduced along the enclosed soil boundary so that no fluid crosses the boundary. The contribution of partially saturated soils and matric suction, as well as the change in hydraulic conductivity due to seepage, are predicted well by the present model. The predicted time evolution of slope stability and seepage induced collapse are in reasonable agreement with the experimental results for homogeneous non-cohesive sand and multiple layered cohesive soils. Rapid drawdown over a sand soil is also investigated, and the location and time of the levee collapse occurrence are well captured. A toe erosion model is incorporated in the BMM model, and the location and quantity of erosion from lateral seepage flow is well predicted. The interplay of erosion, seepage and slope instability is examined.

Keywords: Particle method, levee stability, slope instability, levee Collapse, Seepage Erosion, erosion

1. Introduction

Water plays a significant role in the ability of a soil to maintain its shape under a variety of loadings and conditions. Seepage in particular, is often poorly represented in numerical models, therefore, its erosive power is neglected entirely. The structural integrity of levees, rear sides of breakwaters and riverbanks is critical for the protection of life and assets. Riverbank erosion alone has been recognized as a problem of global significance [1]. It is therefore crucial to establish an accurate model prediction of soil slope stability under seepage conditions

The stability of river banks, levees and other such soil slopes has received much attention in the past. Since Slope/W [2], General Limit Equilibrium and Finite Element Methods of modelling slope stability have been used widely as engineering design tools to predict the safety of these slopes. The majority of these models compute the factor of safety (*FoS*) of a soil slope based on the limit equilibrium of rotational or translational failures of the soil body, by dividing the mobilised slope up into slices or wedges [3-5].

An alternative to experimental observations of FoS is an equilibrium model such as the Discrete Element Method (DEM). This method uses a mass-spring contact between soil particles and considers the movement of soils at a particulate level. This interparticle force is the key driver behind the entire model output, and is not based on traditional soil strength values, but rather back-analysed functions [6]. This method is adpted by many commercial codes, for example Particle Flow Code (PFC) which can be used to model the movement of a slope. The particle nature of this model makes it highly adaptable to scenarios of high strain, however the mechanics of the model make it difficult to produce detailed Factor of Safety predictions

The slope stability problem is further complicated by the presence of seepage, erosion and undercutting caused by surface water. A partner program to Slope/W, SEEP/W developed by Krahn [7], incorporates the movement in the water table, as well as dynamic pore water pressures, in the slope stability analysis. This and

- Corresponding authors: E-mail: johan.vandamme@plymouth.ac.uk (J.Vandamme)

other slope stability models use computational meshes fixed in space. They become unstable and inaccurate when the high strain caused by large relative movement, or significant erosion, is present. Two dimensional seepage often generates erosion and undercutting throughsurfacing water. This has been investigated by Chu-Agor et al. [8, 9] where a null region without soil strength is artificially created to emulate the effect of removed soil properties.

The effect of seepage is important to identify for a number of reasons. Seepage may reduce the effective stress of surface soil particles to zero (liquefaction), leading to erosion and episodic collapse of the bank [10]. The seepage affects the bank stability through the combination of toe erosion and loss of soil suction that reduces the restraining forces on the soil slope, or an increase in soil weight and pore water pressures that further increases the mobilising forces on the soil slope. In some cases, falling external water tables cause a loss of containing pressure when the water level recedes [11].

Negative pore water pressure, known as matric suction, causes an apparent cohesion that significantly increases the slope stability. The loss of this matric suction when the soil within a bank is saturated, significantly reduces bank stability, and thus may trigger bank failures or episodic collapse [12].

Inundation of the soil by rainwater or lateral seepage has been identified as an important factor in the stabilities of banks, slopes [13], bluffs, breakwaters [14] and levees. The particle based Bluff Morphology Model was originally developed to analysed the stability and collapse of static slopes and coastal bluffs by Vandamme et al. [15]. In this paper, we will extend this particle method for slope stability by incorporating the key soil parameters related to seepage and erosion described above and multiple soil types. The model results are compared to the laboratory experiments and the outputs of the Finite Element Model Slope/W. The aim of this paper is to investigate the change in slope stability, and the mechanisms and times of collapse of soils induced by two dimensional seepage.

2. Extension of Particle Based Bluff Morphology Model

The particle based Bluff Morphology Model [15] combines a multiple wedge displacement method with an adapted Weakly Compressible Smoothed Particle Hydrodynamics (WCSPH) method. At first, the wedge method is applied to compute the stability of the bluff. Once the critical failure mechanism of the bluff slope has been identified, and if the factor of safety for the mechanism is less than 1, the adapted WCSPH method is used to predict the failure movement and residual shape of the slope. This model is extended to incorporate the seepage, erosion and undercutting in this section.

2.1 Stability Evaluation

The model set-up uses a hexagonal particle tessellation when considering a static earth profile. Hexagonal tessellation is used as it is the most spherical particle shape that still tessellates It allows for the best approximation of truly 2D movement of the fluid and the failure plane analysis to operate with less complication. Once failure has been shown to occur, the failure mechanics require the adoption of a spherical (or near spherical) particle to avoid complications with angular particle interactions and their associated complexities. These particles are arranged in order to best represent the soil profile, and then assigned a set of scalar parameters including mass, pore water pressure, position, and earth material properties. It would be theoretically possible to assign an individual set of earth material strength properties to each particle within the model, although this would significantly slow the analysis down. Different from [15], multiple soil types are considered with each particle representing one of the soil types in this paper. Each soil type is taken as homogenous within its boundaries, and there is no variation in the individual soil properties within its boundary.

In order to assess the stability of a soil slope, the model uses a displacement-stepping wedge method based on the concept of McCombie [5], and detailed in [15]. This allows for a variety of potential slip surfaces to be analysed, in particular, from large rotational failures to linear translational failures. The conceptualised cycle mechanism to find the failure surfaces is shown in Fig. 1. Initially, the method assumes an entry point of an arbitrary failure surface on the soil surface, and then an exit point above this. Many potential slips that fit these two points are then analysed, from linear to a near-circular analysis where the back of the potential

failure surface is vertical (steps 3 and 4 in Fig. 1). If the slip surface daylights (point A), then the entry point is moved to the appropriate place. The exit point is then stepped across the domain repeating this loop, and then the entry point is moved and the loop begins again.

Once the analysis of each slope is completed, the Factor of Safety along the slope boundary is computed. This in turn can be assigned to the particles on the boundary of the slope, and each particle retains the lowest Factor of Safety assigned to it over many potential slip surfaces. This procedure provides the spatial distribution of factor of safety of the entire slope at any given time.

Each soil used in the model is defined by the strength parameters of cohesion (c') and internal angle of friction (ϕ'), as well as the effective stress (σ'), unit weight, permeability and porosity. This is based on the Smoothed Particle Hydrodynamics (SPH) particle model which saves computational time and reduces memory demand, each model particle is taken to represent an area of single soil using the Mohr-Coluomb shear profile. The values of these parameters are taken from the average laboratory experiments of the given soil. The shear strength τ may be calculated using the following formula, if the soil is fully saturated, or completely dry:

$$\tau = c' + \sigma' \tan(\phi') \quad (1)$$

The slope stability model uses a displacement stepping algorithm, where the mobilised cohesion and the angle of internal friction are increased incrementally and proportionally with the strain along the boundary of the mobilising soil until the shear strength matches the mobilising force. The strain itself is only computationally significant if soils mobilize at different rates, or if the output of the strain is extrapolated as a failure model. The ratio of maximum shear strength to the shear strength required for stability is defined as the Factor of Safety.

Where multiple soil types exist in the same wedge boundary, the model calculates the shear strength pro-rata to the proportion of soil types. These soil types do not have to reach peak strength at the same time for the computation to work. Due to the numerical averaging of the soil types, increasing the number of wedges in each potential slip surface allows for greater accuracy of the shear strength, however it also increases the computational time required. In this paper, analyses were performed using 6-12 wedges per slip which was found to be sufficient for the present study.

The minimum Factor of Safety of each particle along the base of a potential failure surface is stored, and after all potential failure surfaces have been analysed, the model produces a cross-sectional diagram of the Factors of Safety, showing a stability map of the slope.

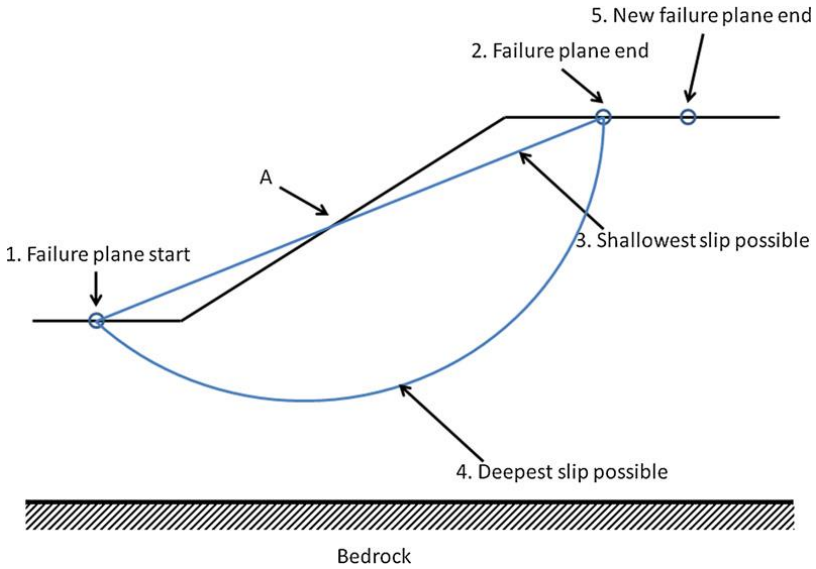

Fig. 1 – Conceptualised cycle of Bluff Morphology model (BMM) mechanism to find failure surfaces.

2.2 Seepage Analysis

This paper presents the two dimensional seepage analysis of the BMM, using Darcy's Law across neighbouring particles, as seen in Fig. 2. Given the initial hexagonal placement of particles, each particle must be analysed for seepage in six directions at each time step. The time steps are small enough to avoid unphysical emptying of voids during any single time step. Darcy's Law is thus applied:

$$Q = k\frac{\delta p}{\delta l}A \tag{2}$$

$$\Delta Vol = \frac{Q\,dt}{V_p} \tag{3}$$

Where k is the minimum permeability of the two particles considered, δp is the pressure differential over the distance (δl) between particles, and A is the cross sectional area between particles. This flow rate is converted to a dimensionless volume of water by multiplying by the time step, dt, and dividing by the volume of each particle. As a two dimensional model, we consider all variables in term of a unit thickness in the third dimension (depth).

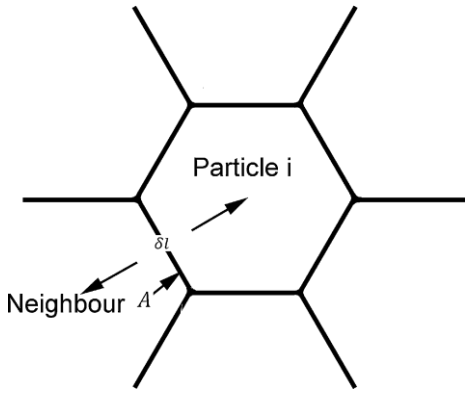

Fig. 2 – Diagrammatic representation of particle tessellation, where neighbours are δl distance apart, and seepage flows over a boundary of area A

The movement of air within the model is considered as the result of a fixed void space and the movement of fluid into the voids. Therefore, the air volume within the model particle is always defined to fill any remaining void space following the pore water movement.

In order to ensure accurate boundary conditions are satisfied, the model creates ghost particles along the enclosed boundaries of the earth material. These ghost particles play a similar role to the Smoothed Particle Hydrodynamics ghost particles (for example, see [16]). They reflect the pore water pressures of the soil particles along the boundary and ensure that no fluid crosses the constrained fluid boundary. Open boundaries are modelled as air particles that the soil can interact with. Any fluid that seeps into these air particles is immediately discharged, and a sum of the fluid in these particles indicates the total quantity of fluid exiting the soil.

The application of a particle model to seepage also considers the effect of Matric Suction on partially saturated soil particles. The contribution of suction are included based on the proportion of water within each soil particle, and as such disregards whether the soil is wetting, or drying following [17]. This suction reduces the permeability (hydraulic conductivity), as shown in Fig. 3. The soil water characteristic curve and permeability functions used within the model are a simplified version of the constitutive equations of [17], assuming homogeneity and isotropic conditions within the soil samples, and are shown in Fig. 3.

Including matric suction in the strength formula of (1) gives the formula of Fredlund et al. [18]

$$\tau = c' + (\sigma - u_a)\tan(\phi') + (u_a - u_w)\tan(\phi_b) \tag{4}$$

where σ is the total stress on the soil, u_a is the air pressure, u_w the water pressure, and ϕ_b the angle of matric suction, which is typically between ten and twenty degrees [19].It should be noted that for a saturated soil, the equation reduces to (1), as ϕ_b attains a maximum value of ϕ' under saturated conditions [20]. In this model, ϕ_b is taken as a constant and the strength of a saturated soil is computed using (1).

At constant time intervals, the seepage analysis is paused until a stability analysis is completed. This allows a comprehensive evolution of stability with time as the seepage significantly alters the soil strength in a complex two dimensional way.

2.3 Erosion & Undercutting Effects

The Bluff Morphology Model incorporates the prediction of erosion in this paper in two different ways. Firstly, in addition to this method of following pre-predicted erosion, the model also checks for particles stability with an inbuilt liquefaction model, using a modified shear strength formula.

$$\Psi = c' + \sigma' \tan(\phi') - \{\Delta\sigma' + \Delta u\} \quad (5)$$

Where $\Delta\sigma'$ represents the difference in horizontal earth stresses, and Δu the difference in the horizontal components of the water pressures on either side of the particle. If Ψ is negative, the disturbing forces on the particle are greater than the restoring forces, and the particle is unstable, and hence it is removed. The pore water within the soil particle is considered to be held within the soil and is removed from the domain with the particle. With a reasonable resolution, the volume of the removed soil and water is negligible compared to the overall domain, therefore, for the scenarios examined in this paper, the conservation of the water mass is not of concern.

Should a particle be removed from alongside an external boundary, the ghost particles are re-generated to ensure the boundary is adjacent to the model soil particles. The pore water pressure of the ghost particles is generated at each time step to mirror the soil particles above, so any erosion is only considered at the end of each time step to ensure no feedback arises.

Secondly, the Bluff Morphology Model predicts earth material erosion through the stability method. Once seepage erosion happens, small failure events often start to develop within the bank. These failures are usually small enough to be classed as undercutting, as opposed to episodic collapse, and occur before the catastrophic failure event of the bank. The developments to the BMM can identify these small failures and subsequently remove the associated particles. These two methods can be used simultaneously, and the authors used the first method of erosion to produce the results in the rest of this paper, as the second method, even when applied, was found to not occur. This is probably due to the resolution of the models; however the impact of small scale slips remains an open question.

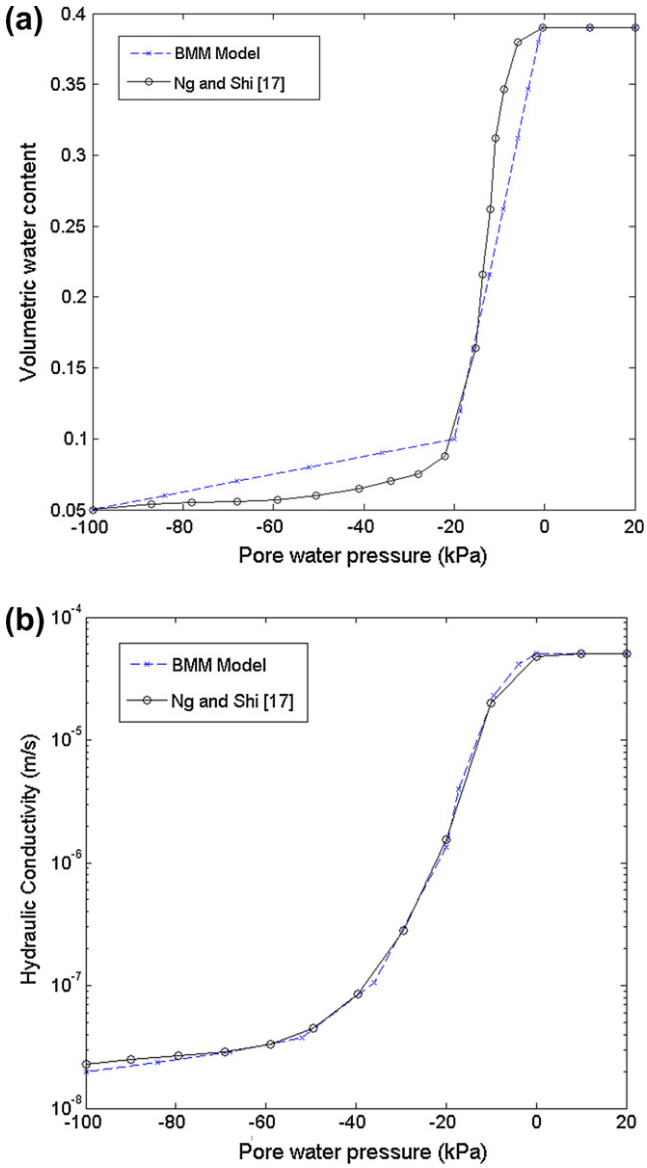

Fig. 3 – Soil Water Characteristic Curve (top) and Permeability function (bottom) relationship to Pore Water Pressure properties used by the Bluff Morphology Model (blue) compared to that of Ng & Shi (black) [17].

2.4 Soil Parameters

This paper seeks to reproduce well documented laboratory tests of slope failure as a consequence of seepage. As a result of this, the soil parameters are considered to be uniform within the individual soil boundaries and the soil properties of the published results are used.

The model simulation requires the cohesion, angle of internal friction, unit weight and permeability of the soils as input parameters. These parameters are gained from the physical parameters given in the publications of the physical tests. The hydraulic conductivity, as seen in Fig. 3, is scaled to the saturated permeability of the soil, and the void ratio of the soils is taken as a constant 60%.

3. Previous Experimental and Numerical Model Results

3.1 Lysimeter experiments of homogeneous cohesionless soil of Fox et al. [19]

The set up of these experiments is illustrated in Fig. 4. The inflow reservoir is kept at a constant height of 30cm, allowing lateral seepage to propagate under constant head boundary conditions. The soil used was a uniform sieved sand, with shear box tests results of c' at 0.25kPa and ϕ' of 35°. The unit weight was approximately 19kN/m^3. Laboratory tests were performed with slope angles of 26°, 36°, 45°, 60° and 90°. Numerical tests were performed with a particle width of 0.008m and approximately 25,000 completed failure planes were analysed during each stability analysis.

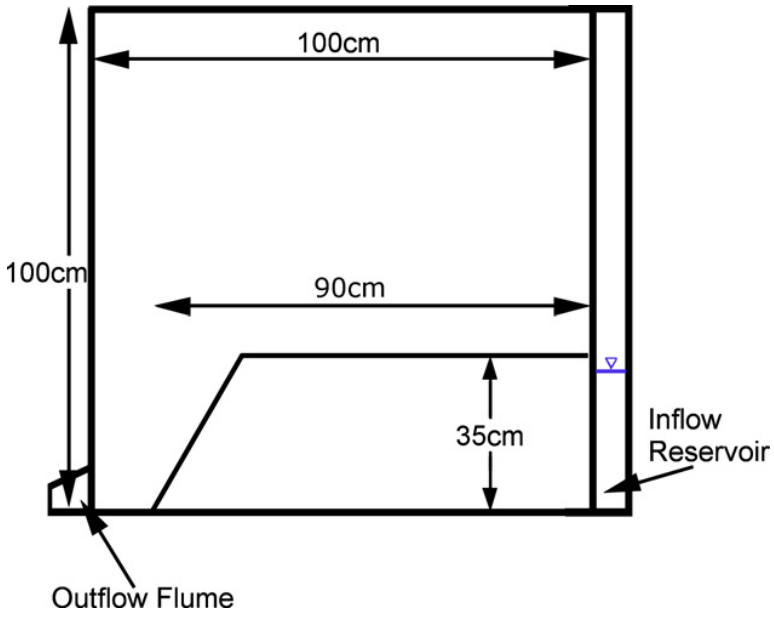

Fig. 4 – Typical set up of the lysimeter experiments of Fox et al. [19]. The water inflow reservoir is at a controlled level and the bank angle is set at 60°

3.2 Lysimeter experiments of inhomogeneous soil of Chu-Agor et al. [9]

Another set of lysimeter experiments were, similar to the experiment of Fox et al [19], but using three different soil layers within the lysimeter. The soil profile is shown in Fig. 10, and is composed of layers of Silt Loam, Loamy Sand, and Clay Loam. The parameters of these soils are given in Table 1 below.

Soil Type	Apparent Cohesion (KPa)	Angle of internal friction	Unit Weight kNm^{-3}	Permeability (ms^{-1})
Silt Loam	7.5	30°	16	1.7x10^{-4}
Loamy Sand	1	25.5°	19	4x10^{-3}
Clay Loam	15	35°	21	1.5x10^{-5}

Table 1 – summary of soil parameters from field tests of Chu-Agor et al. [9]

Laboratory tests in this case were performed with varying water heights and slopes of the lysimeter. These tests have been chosen to evaluate the model's ability to account for seepage and erosion through multiple soil beds, account for the change in stability of a cohesive sediment. Numerical simulations were performed with a particle size of 0.01m and approximately 25,000 completed failure planes were analysed during each stability analysis.

3.3 Draw down failure experiments of Budhu and Gobin [21]

Finally the model is verified against the draw down failure experiment. This test involved a slope constructed of cohesionless sand in a tank. The tank is then filled with water to the top of the slope, and the water level is maintained to allow equilibrium pore water pressure throughout the slope. After this point, the water is

drained at a steady rate until the slope failure occurs. The soil parameters in this experiment are an angle of internal friction of 32^{o}, permeability coefficient of $5x10^{-3}$, and a unit weight of $19kN/m^{3}$. This test evaluates the model's capability to predict the effect of inclined seepage flow with variable boundary conditions, instead of lateral seepage flow under steady state boundary conditions of the previous cases. Numerical simulations were performed with a particle width of 0.045m and approximately 15,000 failure planes were analysed during each stability analysis.

4. Model Validation

4.1 Seepage of homogeneous soil

Fig. 5 shows the progression of the wetted front across a uniform, homogenous sandy bank. The model uses the same parameters and dimensions as the lysimeter experiments of Fox et al. [19]. The saturated particles of the model, shown in red, are considered saturated as their pore pressure is positive, and thus there is no effect of matric suction and no significant volume of air within the soil.

The predicted profile of the wetting front (right panels) that divide the saturated and unsaturated soil, progress with time in the same fashion as the experiment (left panels). These wetted profiles are a curved, near linear profile with a slope that decreases with time.

The difference between the model and the experiment grows with time. The predicted profile by the Bluff Morphology Model is slightly more linear than the experimental data. However, the distance travelled along the base and the top of the sand bank, are identical. The cause for the discrepancy will be discussed in Section 5.1.

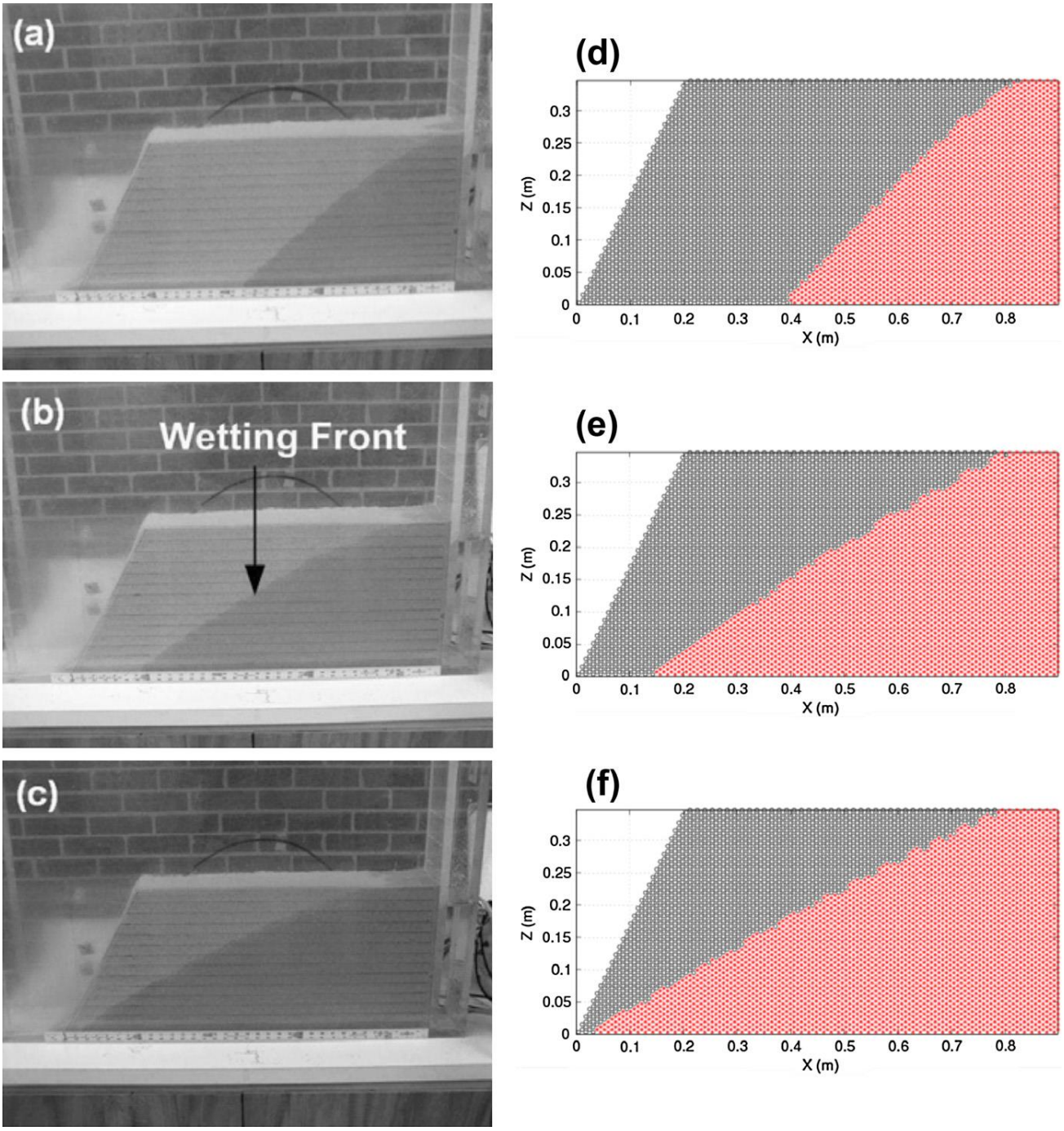

Fig. 5 – Diagram showing the propagation of the wetting front across a sand bank. BMM model on the right (saturated particles red, unsaturated black), with experimental photos from [19] on left.

The model predictions are implemented with a varying modelling particle size/resolution in Fig. 6. Due to the particle based approach of the model, the water content of model particles is responsible for the resultant water pressure, as shown in Fig. 3. As a result, it is important to know the sensitivity of the model resolution to the total seepage volume, which is controlled by the water pressure of neighbouring particles.

As can be seen from Fig. 6, the initial and final water content of the entire soil bank are comparable for a ranged of resolutions, with the variation of the final volume less than 1.1%. As the resolution decreases, the rate of water absorption appears to slow down, producing a smoother and more refined curve for the 0.006 m

resolution (where each particle occupies an area of 31mm^2), implying the finer resolutions offer a more accurate seepage prediction. The result also suggests that a steady state seepage is predicted.

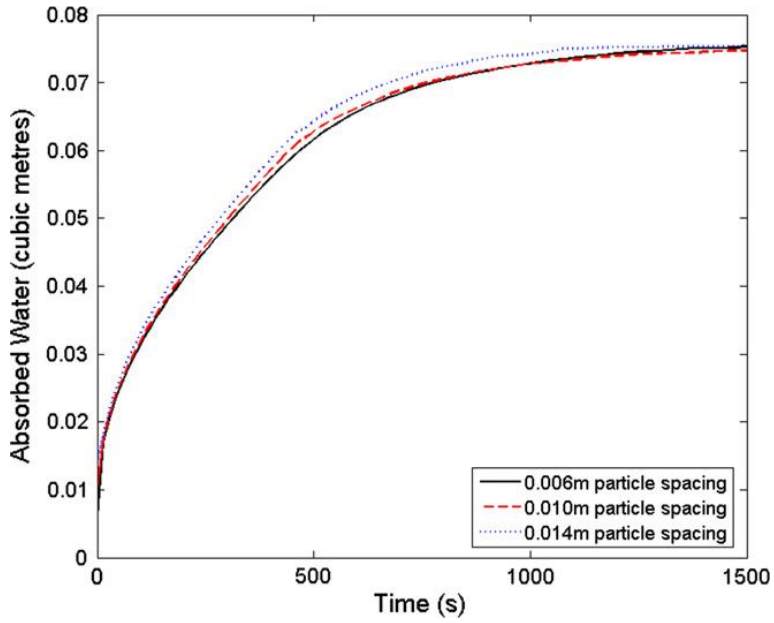

Fig. 6 – Model predictions of Cumulative Seepage using a spatial resolution between 0.006m and 0.014m.

The consistency in Fig. 6 for a significant range of particle size indicates the reliability of the prediction of the seepage rate and the pore water pressure distribution for a dynamic two dimensional seepage case. This is likely to be a result of the model time step which requires maximum volume of seepage flow per model step to stay below the volume of voids in each model particle.

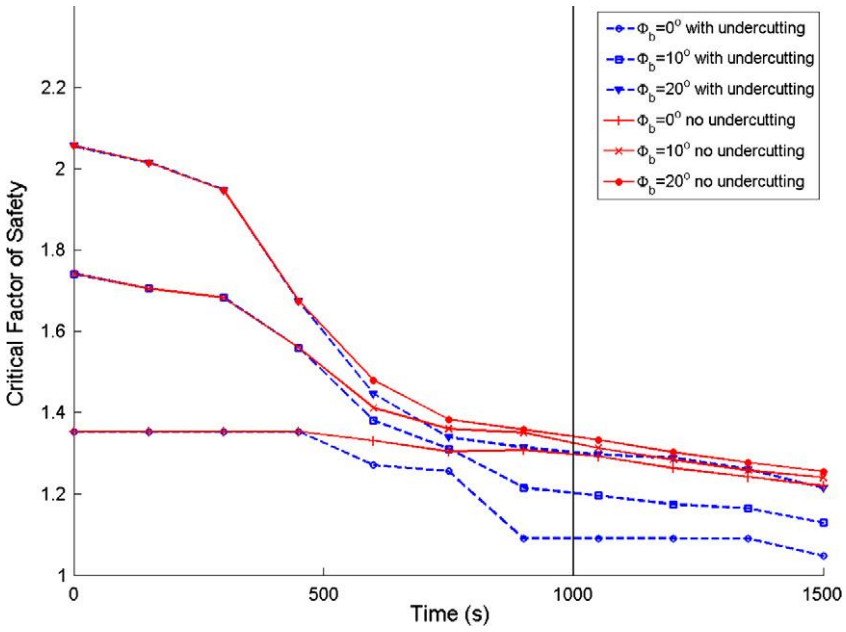

Fig. 7 – BMM predictions of the change in the critical Factor of Safety over the course of 1500s of seepage for a sand bank during the lysimeter experiment of Fox et al. [19]. Time of observed experimental failure given by line at t=1000s.

Fig. 7 shows the variation of the critical Factor of Safety over the course of the lysimeter experiment of a homogenous sandy soil [19]. The soil parameters are given by the shear box test, and results for three values

of ϕ_b, with and without erosion are presented. The expected downward progression of the slope stability as the water seeps through the sand is clear in Fig. 7. This is due to the additional water pressures, reducing the maximum resisting shear force (Equation 1), and the increased weight of the weight soil. The large variation in initial Factor of Safety is caused by the value of ϕ_b chosen, and the respective increase in matric suction (Eq. 4).

The Factor of Safety is slightly over predicted by the BMM, as the experimental results recorded a slope failure at t=1000s. The authors believe the overprediction is due to the use of the shear box test results of soil strength parameter, where the soil was possibly not as well compacted, or as strong in the Lysimeter apparatus. It is also possible that the cohesion recorded in the shear box test was an apparent cohesion caused by the soil suction instead of a genuine soil property. The removal of cohesion strength significantly lowers the Factor of Safety.

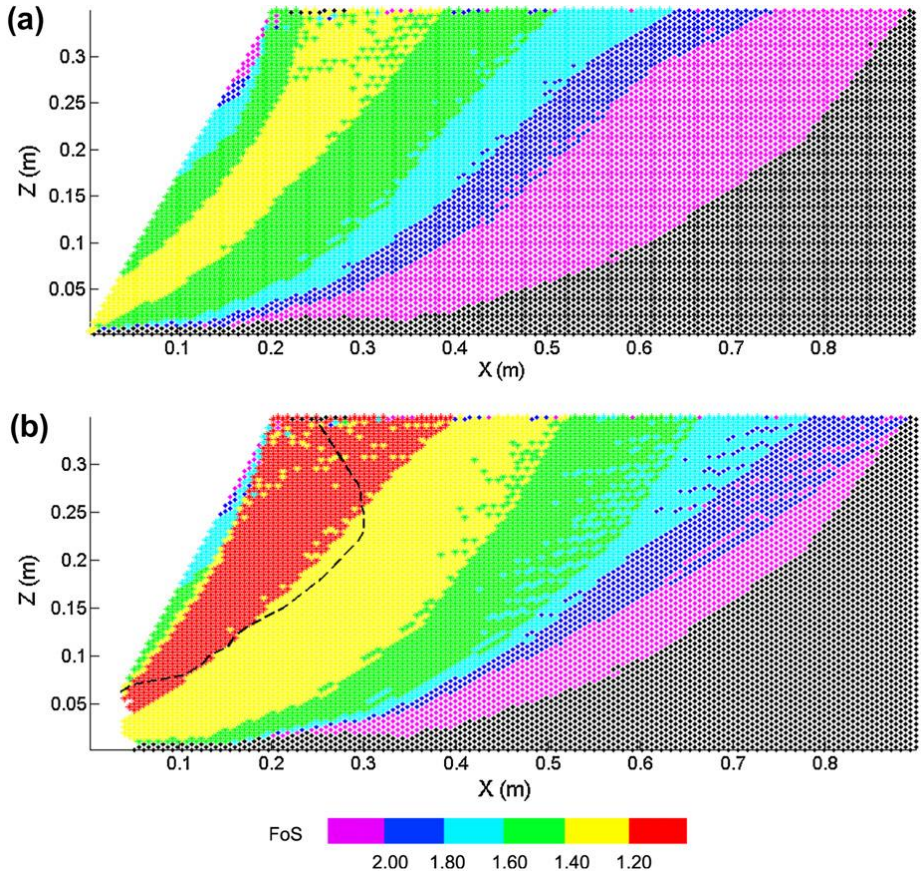

Fig. 8 – Soil Profiles of the Factor of Safety before seepage (top) and after 1500s of seepage (bottom) for the case ϕ_b=0°. Black particles are those with no Factor of Safety found by the BMM, with observed failure of Fox et al [19] (black dashed line).

Fig. 8 shows the profile of the bank and the Factor of Safety before (top) and after the seepage (bottom) for the case with erosion but without matric suction (ϕ_b=0). It is evident that the particles that are removed by the erosion module in the lower corner of the bank. The depth of the erosion compares well with the experiment results Fox et al.[19], although the location of peak erosion (maximum undercut) is lower in elevation than the experimental results.

The increase of instability due to seepage across the entire bank can be seen in Fig. 8, for a case where no matric suction of the soil is considered. The critical slip mechanism is towards the front of the slope (indicated by the red colour), buried beneath the exposed surface by the cohesion of the soil. Increasing the

matric suction of the unsaturated soil tends to decrease the predicted Factor of Safety, but has little effect on the shape and distribution of instability.

Fig. 8 identifies the critical slip mechanism as a 10cm deep translational failure (indicated by the centre of the red contour), which is similar to the observed failure depth. The experimental results, however, showed an initial failure section breaking away leaving an overhanging crest intact, which must have failed soon after, although this secondary failure is not stated within the literature.

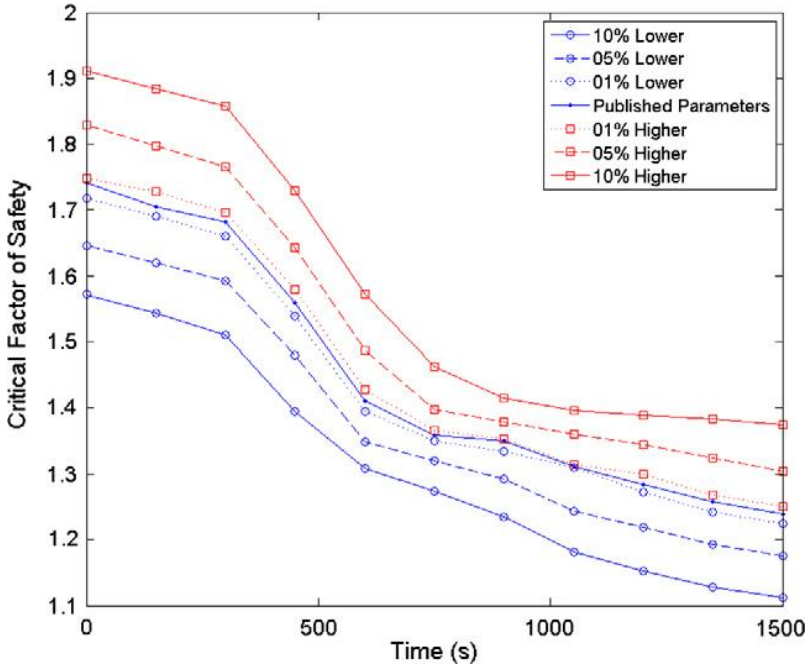

Fig. 9 – Comparison of Factor of Safety for varying the soil conditions for the experiment of Fox et al. [19]

Fig. 9 shows the variation in Factor of Safety over the experiment for various soil strength parameters. The published parameters are for a ϕ_b of 10° without considering undercutting. For a variation of $\pm 10\%$ in the soil strength parameters, we found the critical factor of safety trend mirrored by the varying strength parameters. The percentage error in the FoS is similar but usually slightly lower than that in the strength parameters. This variation gives a reasonable confidence limit of the stability of the soil profile.

4.2 Seepage through non-homogeneous soil

The model is used to study the evolution of the critical factor of safety with time, in a non-homogenous, highly cohesive soil for two cases; with and without undercutting. The results are compared with the lysimeter experiment of Chu-Agor et al. [9] for three soil layers of different permeabilities and different strengths, the numerical set up of which is shown in Fig. 10. The soil profiles in this studyare considered to reach their respective peak strengths at a given strain, as no other data was available to correlate this with.

The initial critical stability is shown to be highly dependent on the value of the matric suction (ϕ_b), however the variance is not as pronounced as in the non-cohesive soil case in Fig. 8. This is because the predominant strength of the soil comes from the cohesion and the pore water pressure has a lesser effect on the stability of highly cohesive soils.

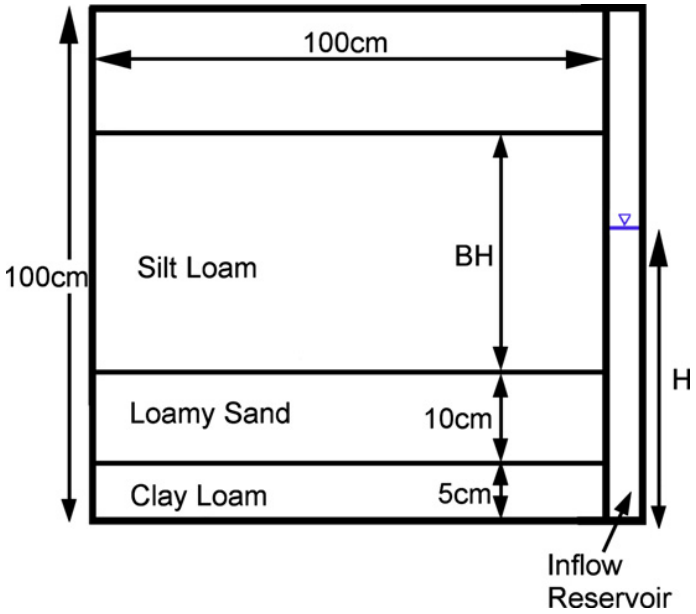

Fig. 10 – Soil Profile of lysimeter experiments by Chu-Agor et al. [9] The water level is kept at a constant height H, and the depth of the Silt Loam layer (BH) varies with different experiments

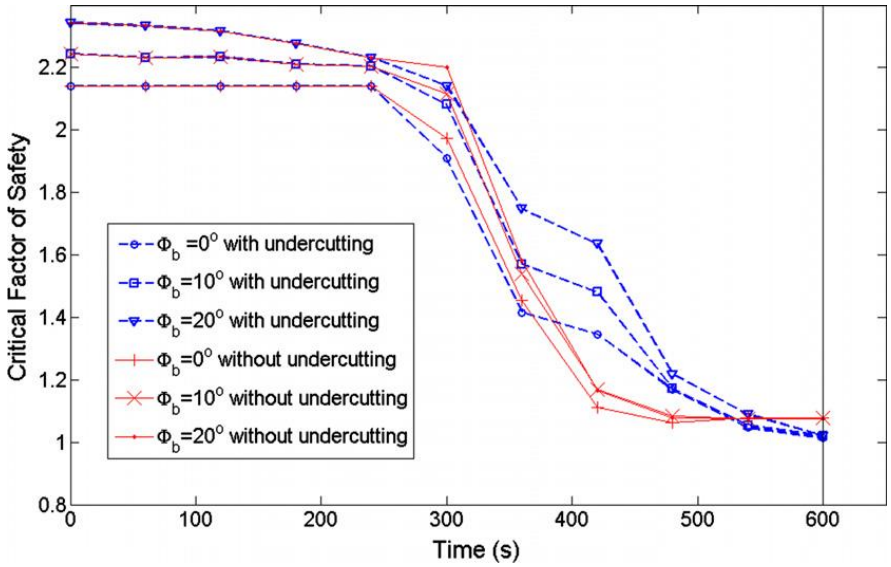

Fig. 11 –BMM predictions of the change in the critical Factor of Safety over the 600s of seepage for a non-homogeneous layered cohesive lysimeter experiment [9]. Time of observed experimental failure given by line at t=600s

The BMM predicts that the stability is significantly altered by the seepage of the water through the soil, in contrast to the Slope/W results of Chu-Agor et al. [9]. This progression is shown in Fig. 11 for the six different cases used. This is likely to be due to a combination of the frictional component of the shear strength being reduced by the pore water pressure, and also the increased weight of the saturated soil. In all cases considered, the variation of the critical Factor of Safety for the slope converges over time, regardless of the value of matric suction, but are different with and without undercutting. In Fig. 11, we can see the effect that erosion and undercutting have on slope stability. The predictions without undercutting appear to maintain a stable soil profile, compared to those with undercutting, where the soil is predicted to transition towards an unstable slope at approximately 610s. The eroded profile predicted by the present model is therefore in reasonable agreement with the experimental results where a slope failure was recorded at 600 s.

A comparison of the erosion predicted by the Bluff Morphology Model to the predetermined erosion used in the computational models of [9] can be seen in Fig. 12. The predetermined erosion of [9] was chosen to match the observed experimental results at five points during the experiment. Fig. 12 shows a smoother profile predicted by the present extended BMM, where the majority of the erosion starts slightly later than the models of [9], but both models approach similar final values that compare well to the observed erosion of the experimental procedure. Neither the experiment nor the model observed any erosion in the cohesive sediment layers.

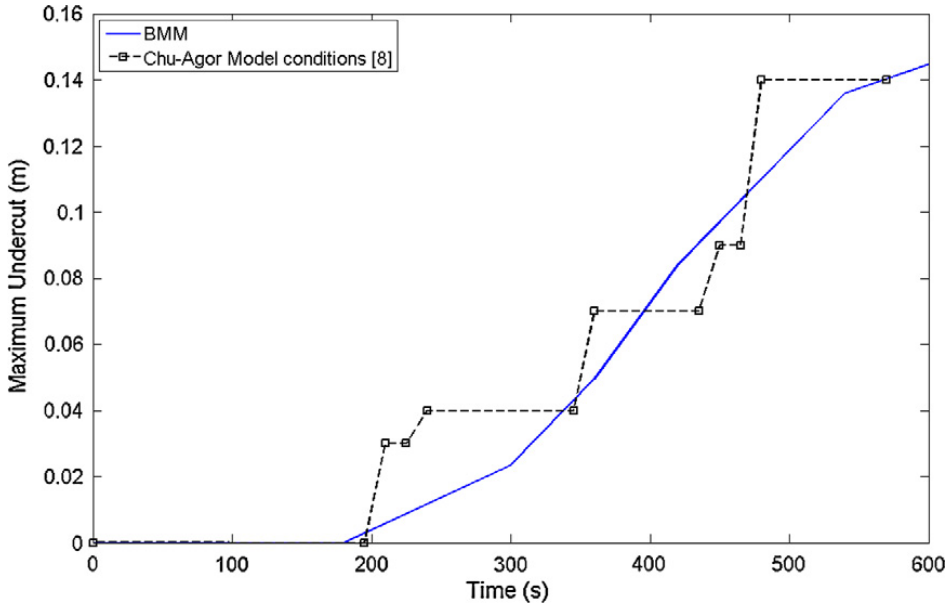

Fig. 12 – Maximum undercut of the Bluff Morphology Model, compared to the conditions used by Chu-Agor et al. [8]

Fig. 13 shows the critical FoS as a function of erosion/undercutting for three the angles of matric suction ϕ_b. The model results were fit to an exponential best fit line for the experimental results of Chu-Agor et al. [9], and have R^2 values of 0.950 and 0.906 respectively, and indicate the expected progression of the critical slope stability over the course of erosion due to the seepage. These results indicate that erosion reduces the stability at the toe of the failure surface where the soil is removed and the soil contact is reduced so is the restraining force on the soil. As a result, the soil mass above the toe becomes largely intact and generate the mobilising force on the soil wedge. After considerable erosion, however, the eroded soil is likely to come from above the failure plane, which reduces the mobilising force. In addition, the erosion is contained within the sand layer, and as the erosion developes, the eroded section propagates horizontally, below the worst case failure planes above.

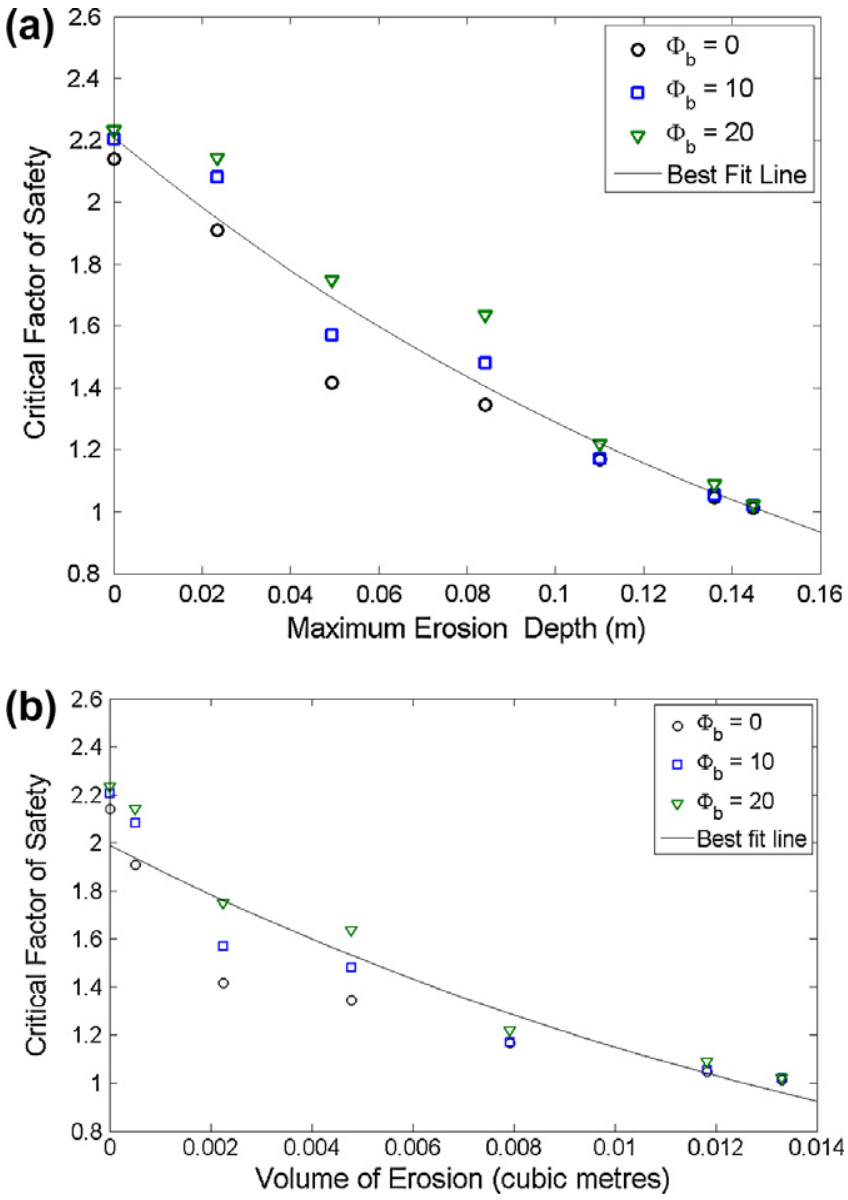

Fig. 13 – The change in the critical Factor of Safety of the soil profile compared to the maximum undercutting depth (top) and volume of erosion (bottom) for the three different values of ϕ_b

4.3 Rapid Draw Down

The model is used to simulate the case of rapid draw down, as modelling a wetting front is relatively simple but the effect of drawdown is more complex. In this example, the soil slope was constructed at 32°, the tank flooded and a constant water level maintained until the soil is fully saturated and the pore water pressures are hydrostatic. After this, the external water level was lowered by 1.667mm/s to match the experimental procedure of [21], until either the tank emptied, or failure occurred.

For this soil, the failure occurred at 411s after the first water level drop. The BMM predicted slope failure at 405s, and the positive pore water pressure distribution can be seen in Fig. 14. The highly permeable sand is draining the pore water out through the front face, and the inclined pressure distribution indicates the rate of change of pore water pressure decreases with increasing distance to the open boundary.

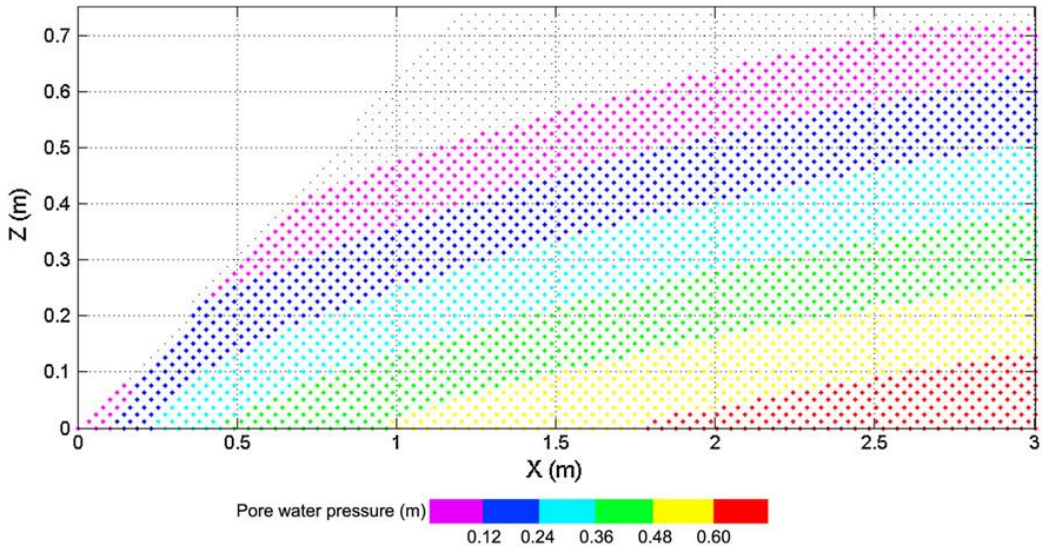

Fig. 14 – Pore water pressure profile of a sand bank after an initially saturated profile is exposed to 405 seconds of rapid draw down

It is evident in Fig. 14 that the boundary particles below 0.08m in elevation are still saturated. This is due to the linearly decreasing water pressure on the boundary particles, modelled to a minimum value of zero.

Fig. 15 shows the stability distribution at the same point. The particles in red are those which become unstable, but the exact location of the slip surface is unknown. However, given the fact that the entire profile of the observed failure is enveloped within the red section, the model predicts the size, timing and location of the failure well.

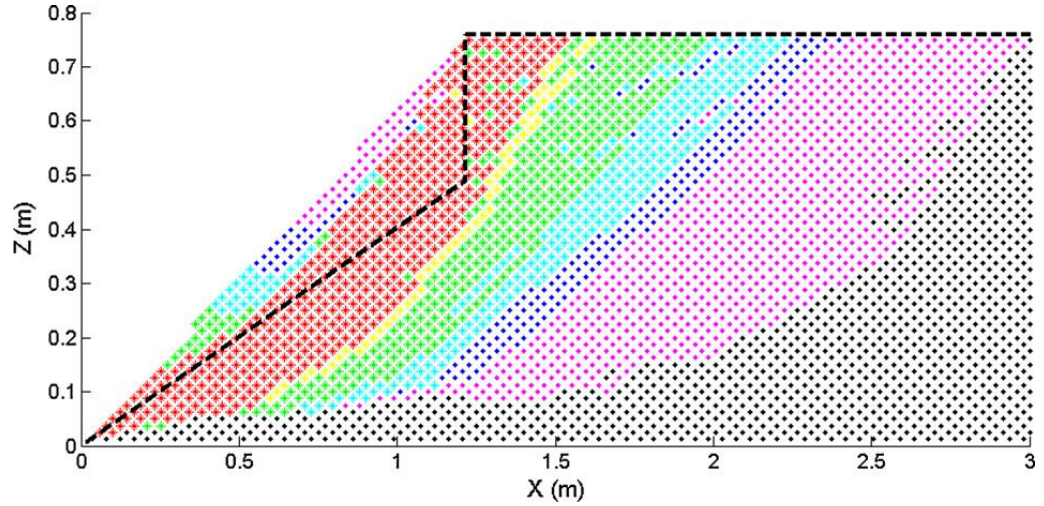

Fig. 15 – Soil Profile of the Factor of Safety at failure. Black particles are those with no Factor of Safety found by the BMM, and the observed failure of Budhu et al [21] is shown in black dashed line.

The over predicted curvature of the failure plane is likely to be due to the matric suction of the partially saturated soil particles. However, it is also evident that there is a probable tension crack in the observations, leading to the vertical face at the back of the slip surface, which fails following a second draw down on the residual profile [21].

5. Discussion

In this section, the results described previously are analysed and considered with regard to both the experimental data and sensitivity analysis.

5.1 Seepage through Homogenous Sand

The effect of two dimensional seepage and erosion on stability is examined by the model in a simple homogenous soil at a constant slope. This experiment provides the basic tests of the model capability in draw down due to its relative simplicity.

The propagation of the wetting front, as seen in Fig. 5, is a clear indication of the models reliability of the prediction of the quantity of seepage, given the significant similarity between the distances the wetting front travelled during the various time steps. In this case the saturated particles were those deemed to have a positive water pressure – i.e. a volumetric water content of above 40%, and therefore zero air volume. A curved wetting profile in the experiment may be caused by the variation of permeability with depth, which is not considered in the model, and likely to offer only slight deviations from the predicted results here.

The change in the critical Factor of safety in Fig. 7 shows erosion has a significant effect on slope stability. In the case of a soil with low or zero cohesive strength, erosion effect comes into play through the removal of the retaining "toe" of the slope in Fig. 10. In the experiment of Fox et al [19], the erosion maintains a higher elevation on the slope than in the BMM. This may be caused by the non-physical removal of eroded particles by the BMM. In a laboratory experiment, eroded particles form a 'scree slope' of material at the toe of the slope, preventing the erosion at the very base. Given the model does not perform this function, the higher water pressures and eroding forces at the toe of the slope result in erosion that is more localised at the toe.

Considering the values of ϕ_b within the model shows a distinct contrast between the model results with and without erosion, as seen in Fig. 7. The intact models, with no undercutting, show a convergence of the Critical Factor of Safety as the soil becomes more and more saturated, and the quantity of unsaturated particles, and thus the effect of matric suction decreases with time in the experiment. However, when the erosion of the particles is considered, this convergence of the Critical Factor of Safety for the different values of ϕ_b is less pronounced. This is due, in part, to the shift in the location of the critical failure plane. The experiments with large matric suction show an expected deeper, and more rotational failure slip, compared to a shallower and more translational slip predicted for small matric suction. This is consistent with the concept of matric suction acting in a similar way to cohesion, and the erosion provides a near-vertical toe of the slope that affords a variety shapes of potential failure plane.

The experiment by Fox et al.[19] produced a failure just before 1000s, with a significant volume of material breaking away from the slope between the height of 50 and 250mm, approximately. This left a significant overhang of soil that is likely to have failed shortly after. The critical Factor of Safety of the model does not drop below 1 at this time frame, and is between 1.1 and 1.4 instead, depending on the value of ϕ_b. In addition to the possible variation in shear box test values of strength, the BMM does not consider tension cracking, which may cause the overprediction of stability and is likely to affect the angle at the top of the failure surface, as a tension crack reduces shear strength on near vertical sections of the slip surface to zero.

The volume of the potential failure within the slope surface ranges from 0.012m^3/m for ϕ_b=0, 0.18m^3/m for ϕ_b=10, and 0.021m^3/m for ϕ_b=20. This compares reasonably well with the recorded experimental mobilised volume of 0.010m^3/m, which rises to 0.017m^3/m when the overhanging soil is included.

Discrepancy between the model and the experiment is typically less than 10%. Considering the variability in soil parameters, this is a good model accuracy. Fig. 9 shows the variation in computed Factor of Safety for a range of the soil parameters, for the case of $\phi_b = 10$ without erosion. The clustering of all Factor of Safety predictions offers a degree of confidence that the output of the model is not skewed by error in the input data due to potential limited experimental accuracy.

5.2 Seepage through Non-Homogenous Soil

The highly permeable layer of sand is sandwiched between much less permeable clay loam and silt loam (Fig. 10), therefore, the water first surfaced at the exposed face of the sand layer after only 190s. The saturated sand layer also produces a downwards seepage into the lower clay layer, leaving only the upper silt layer with a significant portion of unsaturated material. This results in a highly varied pore water profile across the domain, a scenario closer to the real world applications of this model.

Due to the low permeability in the sand layer, the erosion predicted by the model is entirely contained within this soil domain. The cohesion of the upper silt layer keeps the overhang stable, and the lower clay layer has lower water pressures due to the low permeability, and hence less erosive forces. The depth of the undercut predicted by the model is compared to the void region that was programmed into the model comparison of Chu-Agor et al. [9] in Fig. 12. The Bluff Morphology Model shows a much smoother profile, indicating a more continuous erosion of the sand particles. The void regions in [9] were programmed in as there was no erosion calculation within their model, and so a coarse time step was chosen to reduce computational time. The similarity in the rate and the magnitude of the erosion by their and our study indicates the viability of the erosion prediction in the BMM.

The decrease of the stability in the soil slope is predicted over the course of the seepage by the BMM. In this case, the convergence of the critical FoS for various values of ϕ_b is due to the saturation of the lower soil layers, and therefore reduced the matric suction effect for the these soils. This applies equally to the model runs with and without undercutting. The expected reason for the divergence of the critical FoS for various values of ϕ_b at between t=300s and t=450s is caused by the erosion of soil allowing a greater variation of potential failure planes. The case with a low ϕ_b tend toward a steep linear failure surface, behaving similarly to a non-cohesive soil type, and the case of a high value of ϕ_b will tend toward larger, rotational slips. Without erosion, the lack of overhang offers significantly fewer places for steep linear failure planes to develop at the toe of the slope, and therefore less potential failure planes and more uniform FoS predictions. With erosion, the overhang at the front of the slope offers significantly more varied failure planes and therefore matric suction have more pronounced effects.

The change in the critical Factor of Safety with time for cases with erosion is much less linear in the non-cohesive experiment. This is caused by the vertical face of the slope, as erosion is no longer more likely to be found at the toe of the slope and now particles are removed above the critical failure plane as well as below it. Eroding particle above the critical failure plane decreases the active weight within the failing soil mass, and therefore reduces the mobilising forces in the soil domain. Eventually, the reduction of cohesive strength as a result of the removed particles reduces the critical Factor of Safety to a value that is lower than the case without erosion.

Although the reduction of the critical Factor of Safety is not uniform, this reduction can be related to the depth and volume of undercutting with an exponential function as [9] (Fig. 13). The regression analysis of these two variables shows that the maximum undercutting depth is a more significant factor in the reduction of stability (R^2=0.950) than the volume of removed soil (R^2=0.906). Again, this is because the volume of soil is spread both above and below the critical failure surface and therefore decreases both the mobilising and restoring forces in the analysis, and a larger depth of undercut results in a larger number of potential failure surfaces.

The experimental results saw a failure occur at 600s after the initiation of seepage. The BMM at this instant predicts a critical Factor of Safety of only 1.020, a 2% overprediction (Fig. 11). This is possibly caused by the fact that the continuous soil nature was used in the model, while a more erratic and variable profile with any slip surfaces and scars, as can be found in cohesive soils in the experiment.

The episodic failure of the earth material was predicted by the BMM to be a predominantly linear failure at a rate of 0.07m^3/m, which is close to the observed failure of 0.12m^3/m. The BMM prediction of the failure surface on the upslope and downslope locations matches the experimental results. However, the BMM predicts a near linear slip between these points, whereas the experimental results show a curved and undulating failure plane. This again highlights the need for the consideration of tension cracks in the failure planes.

The model-data comparisons indicate the viability of the BMM. However, the failure planes within the soil mass that are predicted are too uniform, and spatial variability [22] needs to be better represented in future studies.

5.3 Rapid Draw Down

One of the key features from this test run is the stability in the pore water pressures on the right hand side of the slope (Fig. 14). These are not on the open boundary, and thus should remain near constant pressures. Over time, the water will drain across the entire soil domain so that the right hand boundary has reduced pressure. This can be seen in Fig. 14 as a very slight deviation from the surface of the bank. However, the right hand boundary maintains the highest pressure across the domain, and this is indicative of an accurate seepage model.

Despite the highly permeable soil, this test run predicted no erosion from the bank face. Although this may, in part, be due to the resolution of the model, this result is also supported by the way the water surface decreased, allowing the shallow depth of soil to equalise under low differential pressure head.

The prediction of the slope failure at 405 seconds after the initiation of draw down is in excellent agreement with the experiment. In addition, the location of the soil particles of critical instability shows the importance of slope failures below the water level.

The shape of the stability profile of Fig. 15 again indicates the importance of considering matric suction in soils of partial saturation. The critical Factor of Safety is buried below the surface, and the residual angle of the BMM prediction is close to the residual angle of the experimental results, at 10^o lower than the angle of internal friction.

It is very likely that the experimental results have a tension crack in the top face of the slip surface. Although this vertical slope later failed [21], vertical tension cracks is a logical future subject for the model in order to improve results.

6. Conclusions and Discussion

A novel particle method has been constructed to examine the stability of a soil bank and levee under a variety of two dimensional seepage conditions. The model reproduces the change in stability and soil morphology with acceptable accuracy. The seepage affects stability and profile for cohesive and frictional soils differently. The model prediction has less than 10% error.

Matric suction has been incorporated in the Bluff Morphology Model by incorporating the effect of partially saturated soils on the shear strength. A range of angle of matric suction ϕ_b values have been used in the present study, and show an expected effect on the stability of partially saturated soils.

A sand slope has been modelled with a water reservoir behind it, at a constant head. The predicted seepage into the slope and reduction in slope stability by the present BMM rae in good agreement with the experiment. Slope stability, however, is slightly overpredicted. For a low cohesive soil, the angle of matric suction ϕ_b significantly affects the stability of a bank when seepage takes place. In contrast, highly cohesive materials are affected more by the seepage induced erosion than ϕ_b.

Erosion at the toe of the slope is captured by comparing the lateral hydraulic force and the available shear strength. Any unstable particles are removed automatically, which may cause an e due to the lack of a ‘scree’ pile. This may result in an overprediction of slope stability as the loose materials often form a retaining pressure against the remaining slope. We found that the erosion causes a significant change to the stability of the slope and should be included in the modelling of this problem. However the model would be improved if the mobilised particles is kept in the computational domain so that the downward side of the slope has a potential build up of eroded particles, or scree. In the cases presented in this paper, the downward slope of the experiment is freely draining, and the soil particles are small, scree build-up is not a significant factor in the slope stability.

Considering a multi-soil domain with highly variable permeability, the model predicts the seepage, rate of erosion and occurring time of collapse well. The stability of highly cohesive soil is affected significantly by erosion but not by the angle of matric suction ϕ_b. This result is in agreement with the experiment and numerical model of Chu-Agor et al. [9].

We found that the contribution of soil erosion to the critical factor of safety is dependent more on the maximum depth of the erosion than the volume of eroded material. Similar conclusions are drawn by previous studies of levees, banks and cliffs of high cohesive strength where notching is the predominant cause of collapse [23].

Finally, the magnitude, location and time of failure are predicted well for a rapid draw down case. The associated pore water pressure reduction is modelled successfully, with exiting water on the front face and near-constant pore water pressures on the back face of the soil sample.

By including a two dimensional seepage model, the present extended BMM is capable of predicting the spatial distribution of stability, and location and magnitude of failure mechanisms caused by the toe erosion or change in pore water pressures. The prediction will be improved by extending the soil strength domain to include the effect of tension cracking at the top of slopes, which is often a precursor of failure. These seepage related model predictions together with predictions of the failure mechanics and equilibrium position by the original BMM model of [15] allow us to track the full stability section of a slope under any seepage and erosion conditions in the real world.

Acknowledgments

The second author would like to acknowledge the support of the start-up fund provided by the University of Maine at Orono during this project.

References

1. Darby, S.E., D. Gessler, and C.R. Thorne, *Computer program for stability analysis of steep, cohesive riverbanks.* Earth Surface Processes and Landforms, 2000. **25**(2): p. 175-190.
2. Krahn, J., ed. *Stability modeling with Slope/W*. An Engineering Methodology.2004, Geo-Slope/W international LTD: Calgary, Canada.
3. Donald, I.B. and Z. Chen, *Slope stability analysis by the upper bound approach: fundamentals and methods.* Canadian Geotechnical Journal, 1997. **34**(6): p. 853-862.
4. Donald, I.B. and Z. Chen. *Modern wedge methods of slope analysis - their power and versatility*. in *Second international conference on landslides, slope stability & the safety of infra-structures*. 1999.
5. McCombie, P.F., *Displacement based multiple wedge slope analysis.* Computers and Geotechnics, 2009. **36**(1-2): p. 332-341.
6. Calvetti, F. and R. Nova, *Micromechanical approach to slope stability analysis.* Degradation and Instabilities in Geomaterials, CISM Courses and Lectures, 2004(461): p. 235-254.
7. Krahn, J., *Seepage modeling with SEEP/W.* Geo-Slope International, Ltd., 2004.
8. Chu-Agor, M.L., G.V. Wilson, and G.A. Fox. *Numerical modeling of bank instability by ground water seepage flow*. in *American Society of Agricultural and Biological Engineers (ASABE) Paper no. 072117*. 2007. St. Joseph, MI.
9. Chu-Agor, M.L., G.V. Wilson, and G.A. Fox, *Numerical modeling of bank instability by seepage erosion undercutting of layered streambanks.* Journal of Hydrologic Engineering, 2008. **13**: p. 1133.
10. Fox, G.A., M.L. Chu-Agor, and G.V. Wilson, *Seepage erosion: A significant mechanism of streambank failure.* Proc. ASCE World Environmental and Water Resour. Congr., Tampa, FL [CD-ROM], 2007: p. 15–19.
11. Simon, A., et al., *Bank and near-bank processes in an incised channel.* Geomorphology, 2000. **35**(3-4): p. 193-217.
12. Simon, A. and A. Curini. *Pore pressure and bank stability: The influence of matric suction*. in *Hydraulic Engineering '98*. 1998. Memphis, TN: ASCE, Reston.
13. Crosta, G. and C. Di Prisco, *On slope instability induced by seepage erosion.* Canadian Geotechnical Journal, 2000. **36**(6): p. 1056-1073.
14. Dentale, F., S.D. Russo, and E.P. Carratelli. *Innovative numerical simulation to study the fluid motion within rubble mound breakwaters and the armour stability*. 2009.
15. Vandamme, J., Q. Zou, and E. Ellis, *A Novel Particle Method to Model the Episodic Collapse of Soft Coastal Bluffs.* Geomorphology, 2011. **138**(1): p. 295-305.
16. Monaghan, J.J. and J.B. Kajtar, *SPH particle boundary forces for arbitrary boundaries.* Computer Physics Communications, 2009. **180**(10): p. 1811-1820.
17. Ng, C.W.W. and Q. Shi, *A numerical investigation of the stability of unsaturated soil slopes subjected to transient seepage.* Computers and geotechnics, 1998. **22**(1): p. 1-28.
18. Fredlund, D.G., N.R. Morgenstern, and R.A. Widger, *The shear strength of unsaturated soils.* Canadian Geotechnical Journal, 1978. **15**(3): p. 313-321.
19. Fox, G.A., M. Chu-Agor, and G.V. Wilson, *Erosion of noncohesive sediment by groundwater seepage: Lysimeter experiments and modeling.* Soil Science Society of America Journal, 2007. **71**(6): p. 1822-1830.
20. Fredlund, D.G. and H. Rahardjo, eds. *Soil Mechanics of Unsaturated Soils*. 1993, Wiley: New York. 517.
21. Budhu, M. and R. Gobin, *Slope Instability from ground-water seepage.* Journal of Hydraulic Engineering, 1996. **122**(7): p. 415-417.

22. Cho, S.E., *Effects of spatial variability of soil properties on slope stability.* Engineering Geology, 2007. **92**: p. 97-109.
23. Kogure, T., et al., *Effect of the development of notches and tension cracks on instability of limestone coastal cliffs in the Ryuukyus, Japan.* Geomorphology, 2006. **80**(3-4): p. 236-244.